The Astrophysical Journal, 973:158 (9pp), 2024 October 1 https://doi.org/10.3847/1538-4357/ad6dfa

The Dustiest Galactic S Stars: Mid-infrared Spectra from SOFIA/FORCAST

Kathleen E. Kraemer[1], G. C. Sloan[2,3], and Ramses M. Ramirez[4]
[1] Institute for Scientific Research, Boston College, 140 Commonwealth Avenue, Chestnut Hill, MA 02467, USA; kathleen.kraemer@bc.edu
[2] Space Telescope Science Institute, 3700 San Martin Drive, Baltimore, MD 21218, USA
[3] Department of Physics and Astronomy, University of North Carolina, Chapel Hill, NC 27599-3255, USA
[4] University of Central Florida, Department of Physics, Planetary Sciences Group, Orlando, FL 32816, USA
Received 2024 March 4; revised 2024 July 26; accepted 2024 August 8; published 2024 September 30

Abstract

We present spectra of 12 of the reddest, and hence dustiest, S stars in the Milky Way, observed with the FORCAST grisms on SOFIA. S stars are asymptotic giant branch (AGB) stars with C/O ∼ 1, so their molecular and dust chemistries are dominated by neither O nor C, often leading to atypical spectral features from their molecules and dust grains. All of the stars in our sample have strong dust emission features at 10–11 μm, but the shape of the feature in most of the stars differs from the shapes commonly observed in either oxygen-rich or carbon-rich AGB stars. Two stars also show the 13 μm feature associated with crystalline alumina. Two have a water absorption band at ∼6.5–7.5 μm, and a third has a tentative detection, but only one of these three has the more common SiO absorption band at 7.5 μm. Three others show a red 6.3 μm emission feature from complex hydrocarbons consistent with "Class C" objects, and in a fourth it appears at 6.37 μm, redder than even the standard Class C hydrocarbon feature. Class C spectra typically indicate complex hydrocarbons that have been less processed by UV radiation, resulting in more aliphatic bonds relative to aromatic bonds. None of the S stars show a strong 11.3 μm hydrocarbon feature, which is also consistent with the presence of aliphatic hydrocarbons.

Unified Astronomy Thesaurus concepts: S stars (1421); Infrared spectroscopy (2285)

Materials only available in the online version of record: data behind figures

1. Introduction

A low- to intermediate-mass star, $M \sim 0.8$–$8\,M_{\odot}$, ejects the bulk of its mass while on the asymptotic giant branch (AGB), ultimately ending its life as a white dwarf with $M < 1.4\,M_{\odot}$. This ejected material will be highly enriched with fresh fusion products, contributing significantly to the chemical enrichment of the Galaxy and the Universe (e.g., E. M. Burbidge et al. 1957; R. K. Ulrich 1973; A. I. Karakas & J. C. Lattanzio 2014; C. Kobayashi et al. 2020). As the ejecta cool, molecules and grains condense, forming a circumstellar envelope that has a rich spectrum of features in the infrared, from which the chemical and physical conditions of the material can be inferred (e.g., H. J. Habing 1996; S. Höfner & H. Olofsson 2018, and references therein).

CO is the molecule that determines the chemistry in the outer envelopes of cool AGB stars because it consumes most of the available C or O, whichever is less abundant. On the AGB, freshly fused carbon is dredged up from the interior, and if the C/O ratio exceeds 1, the chemistry of the gas and dust will change dramatically to reflect that new balance (e.g., I. J. Iben 1974; A. Renzini 1983; G. Wallerstein & G. R. Knapp 1998). Although there is a continuum of C/O ratios in AGB stars, the chemistry of the gas and dust shows a dichotomy. Carbon-rich chemistry dominates in carbon stars and oxygen-rich chemistry dominates most of the remaining AGB stars (M giants), and the mid-infrared spectra of each type reflect this dichotomy with distinct sets of molecular absorption and dust emission features (e.g., J. A. Hackwell 1972; K. M. Merrill & W. A. Stein 1976; P. Cheeseman et al. 1989; K. E. Kraemer et al. 2002; M. Matsuura et al. 2005; P. M. E. Ruffle et al. 2015; O. C. Jones et al. 2017).

S stars lie in the transition between these two chemical domains, with C/O ∼ 1. Because of this, odd chemistry can occur in the stellar atmosphere and circumstellar envelope, as different chemical paths are available due to the lack of both C and O, one of which would normally dominate the chemistry. S stars and their infrared spectra can thus directly probe a chemical regime of circumstellar material that is not present in studies of AGB stars, which focus on either the carbon stars or the oxygen-rich M giants.

While the infrared spectra of these stars are commonly classified as part of the oxygen-rich population (e.g., G. C. Sloan & S. D. Price 1998; K. E. Kraemer et al. 2002), their spectral features are often not those typical of silicate and alumina dust and the associated molecular features (e.g., I. R. Little-Marenin & S. J. Little 1988; S. Hony et al. 2009; K. Smolders et al. 2012). For example, the shape of the 10 μm feature can shift to 10.5 μm, and many lack the 18 μm silicate emission feature altogether. Others show features more typically seen in carbon stars such as complex hydrocarbons (e.g., polycyclic aromatic hydrocarbons, hereafter PAHs) and weak versions of the 26–30 μm feature attributed to MgS (e.g., S. Hony et al. 2009; K. Smolders et al. 2010, 2012). Gaseous SiS bands may be seen at 6.7 and 13–14 μm in absorption (W. Aoki et al. 1998; J. Cami et al. 2009; K. Smolders et al. 2012) and in rare cases in emission (G. C. Sloan et al. 2011).

The samples in those previous spectroscopic studies, however, have generally undersampled the dustiest, i.e., reddest, S stars. We therefore undertook a project using the Faint Object infraRed CAmera for the SOFIA Telescope (FORCAST; Herter et al. 2012) on the Stratospheric Observatory for Infrared Astronomy (SOFIA; E. T. Young et al. 2012) to address this gap. Section 2 describes our source

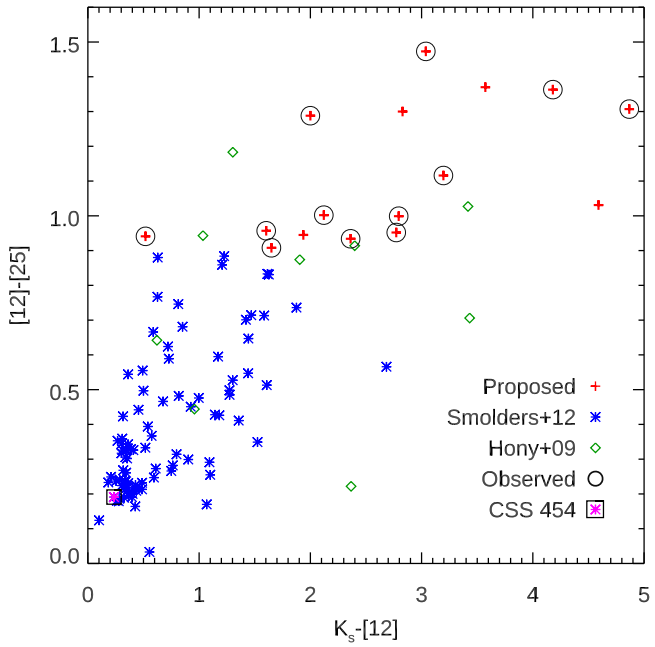

Figure 1. IR color–color diagram for the S star samples with mid-infrared spectra. S. Hony et al. (2009): green diamonds; K. Smolders et al. (2012): blue asterisks; our proposed sample: red pluses; those observed with FORCAST: circles; magenta asterisk with black box: CSS 454, the star used for continuum subtraction in Section 3.1.

(The data used to create this figure are available in the online article.)

selection, the observations, and the data processing. Section 3 describes the results and analysis, and Section 4 summarizes our findings.

2. Source Selection and Observations

Our goal was to investigate the dustiest S stars as these were underrepresented in previous studies. We started with the S stars listed in Simbad[5] and checked the database of P. S. Chen et al. (2019) to ensure we selected intrinsic S stars, i.e., those whose chemical balance is due to the dredge-up of carbon from the interior rather than contamination from mass transfer in a binary. To select the dustiest stars, we used 12 and 25 μm photometry from the Point Source Catalog of the Infrared Astronomical Satellite (IRAS; Neugebauer et al. 1984), complemented by K_s photometry from the 2 μm All-Sky Survey (2MASS; R. M. Cutri et al. 2003). We required [12] $-$[25] > 0.9 as these would be the dustiest stars and are the most undersampled, as Figure 1 shows. Since the K_s-[12] color is not as sensitive to the coolest dust as the mid-infrared color, it was used as the secondary constraint. In particular, we preferentially chose stars with $K_s-[12] > 1.0$; only one of our targets is bluer than this. The IRAS-based colors were compared with those from the Wide-field Infrared Space Experiment (WISE; E. L. Wright et al. 2010), and most (13 of 16) also had $W3 - W4 > 0.9$. WISE-based colors were not used as the primary criterion as these sources are almost all partially saturated in the WISE bands.[6] With one exception, sources that had been observed with the Short-Wavelength Spectrometer (SWS; T. de Graauw et al. 1996) on the Infrared Space Observatory (ISO; M. F. Kessler et al. 1996) were removed from the candidate target list. RW And was retained as a target since its SWS spectrum was too noisy to use (K. E. Kraemer et al. 2002; S. Hony et al. 2009). A lower limit to the 12 μm flux density of $F_{12} = 10$ Jy ensured the required signal-to-noise ratio (S/N) could be reached in reasonable integration times. We also imposed a decl. limit of $-25°$ as FORCAST was not expected to deploy to New Zealand in Cycle 9.

These selection criteria resulted in a set of 16 S stars, of which 12 were observed with the FORCAST grisms under Plan ID 09_0046. Table 1 provides details on the observed targets; those not observed are listed in the Appendix. Eight stars have data from all four grisms: G063 (4.9–8.0 μm), G111 (8.4–13.7 μm), G227 (17.6–27.7 μm), and G329 (28.7–37.1 μm). The other four were observed in at least the G111 grism.

The observations used the two-position chop and nod setting (C2N) with the default 60″ chop throw and 30° chop angle. Integration times were set to achieve S/N > 30 in G063 and G111 and S/N > 25 for G227 and G329 (the features in the redder grisms typically being broader than those in the bluer grisms). All times in G063 were set to 30 s. Those in G111 and G227 were set to 30, 60, or 100 s, depending on the 12 and 25 μm flux density. Those in G329 were set to 100, 300, or 500 s, depending on the 25 μm flux density. These settings would achieve our S/N goals based on the SOFIA Instrument Time Estimator.[7] The G329 grism was omitted for sources with $F_{25} < 15$ Jy. The 4.″7 slit was used for all observations, which results in spectral resolving powers of $R \sim 125$ for G063 and G111 ($\lambda = 4.9$–13.7 μm) and $R \sim 70$–110 for G227 and G329 ($\lambda = 17.6$–37.1 μm).

We use the Level 3 spectra provided by the SOFIA pipeline. The pipeline corrects instrumental effects, extracts spectra, applies the flux calibration, corrects for atmospheric transmission effects, and coadds any spectra taken at the same settings to generate a single spectrum for each grism.

Only the G111 spectral segment required additional processing. For this segment, the atmospheric correction left residuals, notably in the ozone band at $\lambda \sim 9.25$–10.05 μm. Also, the reddest data were usually very noisy due to residual H_2O and CO_2 vapor longward of $\sim$13.8 μm. These spectral regions were therefore masked out individually for each star.

3. Results and Discussion

Figure 2 shows the FORCAST spectra for the observed S stars. The spectra are dominated by a broad emission feature around 10 μm, as expected for this kind of dust-producing star. Several, but not all, show a weak 18 μm feature similar to M giants. Two stars also show the 13 μm emission feature seen in some O-rich AGB stars. At least two stars have an absorption feature from the H_2O band at 6.5 μm, and at least three others have an emission feature from complex hydrocarbons near 6.3 μm. No SiS bands were detected in our sample. The detected gas and dust features were separately isolated from the continuum and characterized, as discussed below.

[5] As of 2020 July.

[6] Only W4 for HD 35273 was unsaturated.

[7] No longer available after the mission ended. The minimum integration time of 30 s was set by the fact that observations this short were dominated by overheads.

Table 1
Source Properties and Observation Summary

Star Name	R.A. (J2000)	Decl. (J2000)	F_{12} (Jy)	F_{25} (Jy)	[12]−[25] (mag)	K_s − [12] (mag)	Spectral Type[a]	Obs. Date (yyyy mm dd)	λ_{obs} (μm)
RW And	11.828799	32.685600	36.1	18.5	0.91	1.65	S6/2e	2022 May 26	5.1–37.1
HD 35273	80.836281	−4.570621	20.0	10.7	0.96	1.60	M4wkS	2022 Feb 1	5.1–13.8
Y Lyn	112.048424	45.990589	121.9	64.2	0.94	0.52	M6S	2022 Feb 8	5.1–37.1
IRC −10401	272.603333	−10.571130	177.4	109.8	1.12	3.20	M7S	2022 Feb 2	5.1–37.1
IRC −10411	275.099243	−14.113032	37.9	27.5	1.29	2.00	S	2021 Jul 9	5.1–37.1
CSS 1055	278.184753	−9.486253	28.4	15.8	1.00	2.79	S	2021 Jul 8	5.1–37.1
IRC −10450	280.056274	−5.703139	124.4	91.8	1.31	4.87	S	2021 Jul 9	5.1–37.1
IRC +00402	284.601105	4.665304	88.2	46.2	0.93	2.36	M2	2022 May 25	5.1–37.1
CSS2 41	294.782379	29.044159	50.4	39.1	1.36	4.18	S	2022 Feb 10	5.1–37.1
CSS 1185	300.791840	29.986435	29.7	15.8	0.95	2.77	S	2022 May 26	5.1–27.9
IRC +60374	343.301422	61.283463	108.5	93.3	1.47	3.04	M3Ib	2022 Sep 14	8.8–13.8
WY Cas	359.505493	56.487099	50.9	28.4	1.00	2.12	S6	2022 Jan 27	5.1–27.9

Note.
[a] From Simbad.

3.1. Dust

3.1.1. Feature Extraction

To isolate the dust features, a stellar continuum was subtracted from each spectrum. We used the Spitzer Infrared Spectrograph (IRS) spectrum of CSS 454, a dust-free S star with relatively weak molecular absorption (K. Smolders et al. 2012; CSS 454 is the magenta asterisk and black square in Figure 1).[8] The IRS spectrum was resampled to the FORCAST wavelength grid of each S star, scaled to the average flux density in the 5.5–7.8 μm range, then subtracted from the target spectrum. Figure 3 shows the resulting residual spectra, which are dominated by the dust emission feature at ∼10 μm.

S stars tend to be slightly O rich due to the traditional identification criteria,[9] so we compared the observed features to profiles from combinations of dust from commonly used oxygen-rich minerals, such as silicates, alumina, and gehlenite. Because C/O is close to 1, we also included silicon carbide (SiC) and amorphous carbon. Dust constants for the silicates were from V. Ossenkopf et al. (1992, hereafter OHM), the alumina constants from B. Begemann et al. (1997; Al_2O_3), the gehlenite ($Ca_2Al_2SiO_7$, used by K. Smolders et al. (2012) for their S star sample) from Mutschke et al. (1998, via the Jena Database of Optical Constants website[10]), the SiC from B. Pegourie (1988), and the amorphous carbon from V. G. Zubko et al. (1996). A grain size of 0.1 μm was used to obtain absorption efficiencies (q) from the complex indices of refraction provided by the references given above; the grain size for the amorphous carbon was 0.3 μm. We compared profiles that combined different amounts of OHM silicates, alumina, gehlenite, SiC, and amorphous carbon to the observed dust features by eye. None of the comparison profiles matched the data particularly well, and the uniqueness of any "match" is questionable. A more complete library of minerals could potentially be used to formally fit to the observed dust features, but the need to consider both oxygen- and carbon-rich minerals would make the uniqueness issue even worse.

We look at the shape of the G227 segment to determine whether or not there is an 18 μm feature present in these spectra. In particular, we look for inflections that could be caused by the red shoulder of the feature, the blue shoulder being in the gap between G111 and G227. Y Lyn shows clear inflections in this segment, which likely indicate an 18 μm feature. These inflections are weaker but probably present in four of the other stars and are noted in Table 2. Other samples of S stars also usually have weak or absent 18 μm features. When present, it often peaks closer to 19 μm than the typical silicate feature at 18 μm (e.g., I. R. Little-Marenin & S. J. Little 1988).

The dust residuals in Figure 3 may contain an underlying component whose lack of subtraction artificially enhances the apparent strength of the emission in the 18 μm region. This component is particularly evident in objects where the dust residuals are stronger above 17 μm compared to those below 15 μm, such as IRC −10450 and IRC −10411, but is likely present in all our sources. K. Smolders et al. (2012) included Planck functions with $T = 500$–4000 K, as well as stellar spectra, to isolate their dust features, probably due to this emission excess, although they do not discuss the fitting process or resulting parameters. Possible carriers for the featureless excess emission could include amorphous carbon or iron grains (e.g., I. McDonald et al. 2010). Another possibility is a poor calibration between FORCAST grism segments. However, Figure 2 shows that the G227 and G329 segments are well aligned prior to subtraction of the stellar component, and G111 and G227 generally are, too. Comparison with the IRAS flux densities at 12 and 25 μm finds that sometimes the values match the spectra, sometimes one does and not the other, and sometimes neither does. This may be due to variability in the stars, but regardless, it does not help address the relative levels of the segments.

Two stars show the 13 μm feature attributed to crystalline alumina (G. C. Sloan et al. 2003; A. Takigawa et al. 2015). As Figure 4 shows, Y Lyn has a strong 13 μm feature, as well as the most distinct 18 μm feature and the H_2O absorption band at 6.5 μm (Section 3.2). G. C. Sloan et al. (2003) found that stars with a 13 μm feature often showed a redder component at ∼19.5–20 μm to their 18 μm feature (e.g., their Figure 1).

[8] The bluest source in Figure 1 from the previous samples is an extrinsic S star and thus not appropriate for a continuum template.
[9] The traditional identification from the ZrO absorption band in optical spectra (e.g., P. W. Merrill 1926, 1929; K. Wurm 1940) skews the known population slightly O rich.
[10] www.astro.uni-jena.de/Laboratory/Database/jpdoc/0-entry.html

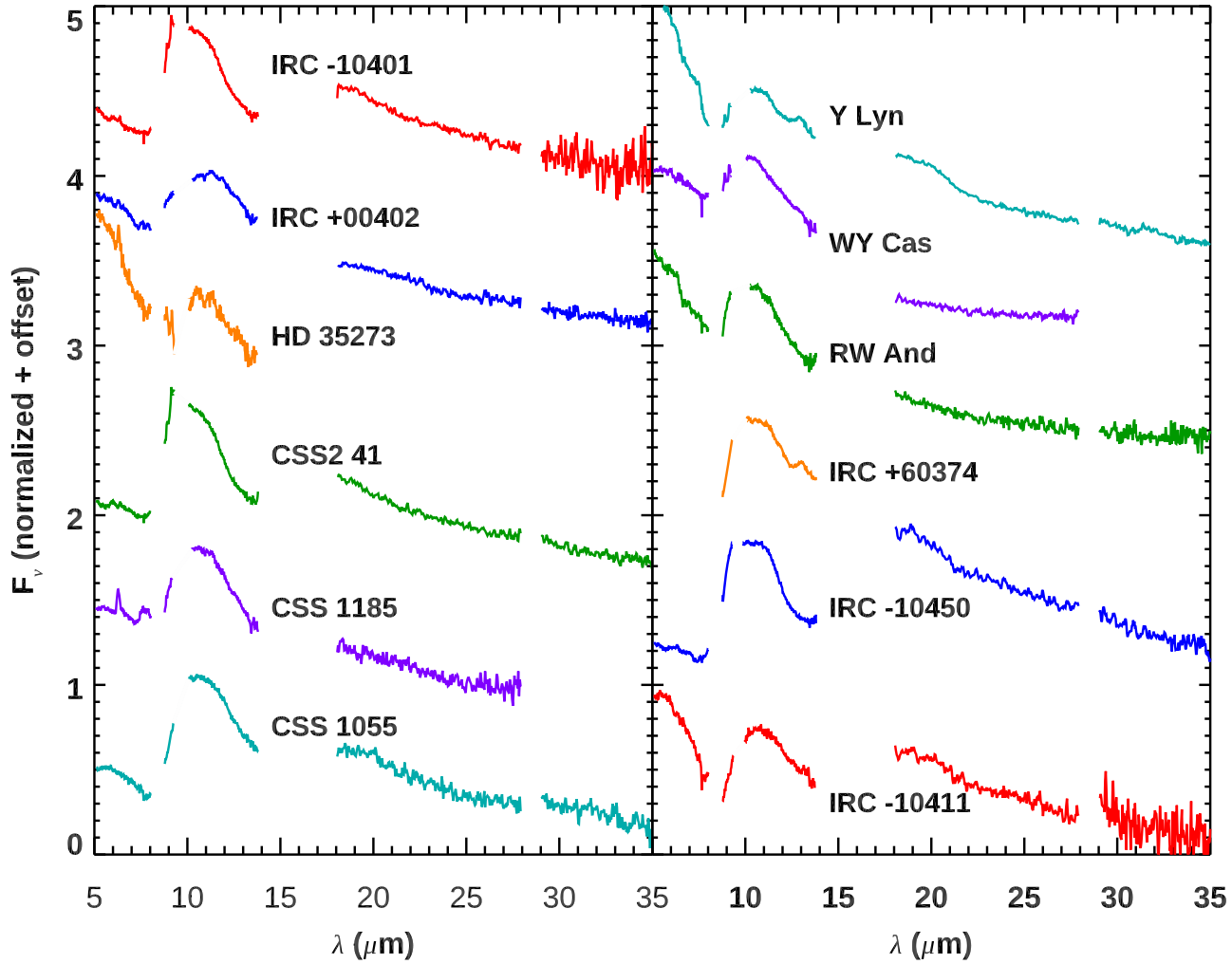

Figure 2. SOFIA/FORCAST S star spectra. The data have been normalized at 10.5–12 μm and offset for clarity. The ~9–10 μm region is grayed out due to residuals from atmospheric ozone, determined individually for each star. A telluric residual is also sometimes present at 7.6–7.7 μm.
(The data used to create this figure are available in the online article.)

While Y Lyn does not have a distinct emission bump at those wavelengths as the oxygen-rich AGB stars often do, its "18" μm inflection is redder than that of the other S stars with tentative 18 μm features but no 13 μm feature, such as CSS 1055. IRC +60374, with the other clear 13 μm feature, only has data from the G111 grating, so it is not known if it has H_2O absorption or an 18 μm feature. WY Cas does have a hint of excess emission around 13 μm, although it is much weaker than in Y Lyn or IRC +60374. IRC −10411 also has excess emission but at a longer wavelength than the typical 13 μm feature.

3.1.2. Dust Emission Classes

The SE classes of G. C. Sloan & S. D. Price (1995, 1998, hereafter SP95 and SP98, respectively) are commonly used to characterize the 10 μm emission feature in O-rich AGB stars, and SP98 suggested that they could be used on S stars. Generally, the spectra from classes with lower numbers, e.g., SE 1–3, have more alumina, and those with higher numbers have more amorphous silicates (SP98 and references therein). Since the SP95 algorithm used to assign the class requires data within the ozone-contaminated region, though, we cannot formally assign an SE class to our spectra (see Equations (4)–(5) of SP98). Instead, we compared the shape of the continuum-subtracted feature to the average spectrum of each class shown by G. C. Sloan et al. (2003) and assign a class by eye. These are given in Table 2, along with the approximate peak wavelength of the emission feature. Figure 4 shows a close-up of the feature. Sources with (roughly) similar features are grouped together.

For several of the stars, the shape of the peak (somewhat) corresponds to one SE class, but the slope to the red, above ~12 μm, corresponds better to the next higher SE class. I. R. Little-Marenin & S. J. Little (1988) had found that the 10 μm features of S stars were distinct from the O-rich AGB stars. S. Hony et al. (2009) also found that the shapes of the 10 μm features in their S star sample differed from those of the O-rich AGB stars. Our data support the suggestion by both groups that the dust composition of the S stars likely differs from that of the O-rich AGB stars.

Two of the stars, IRC +00402 and WY Cas, do not correspond well to any of the SE classes, albeit in different ways. This indicates that their mineralogy differs even more from the standard alumina+classic silicates of O-rich AGB stars (e.g., M. P. Egan & G. C. Sloan 2001) and that they may be relatively more carbon rich than the others.

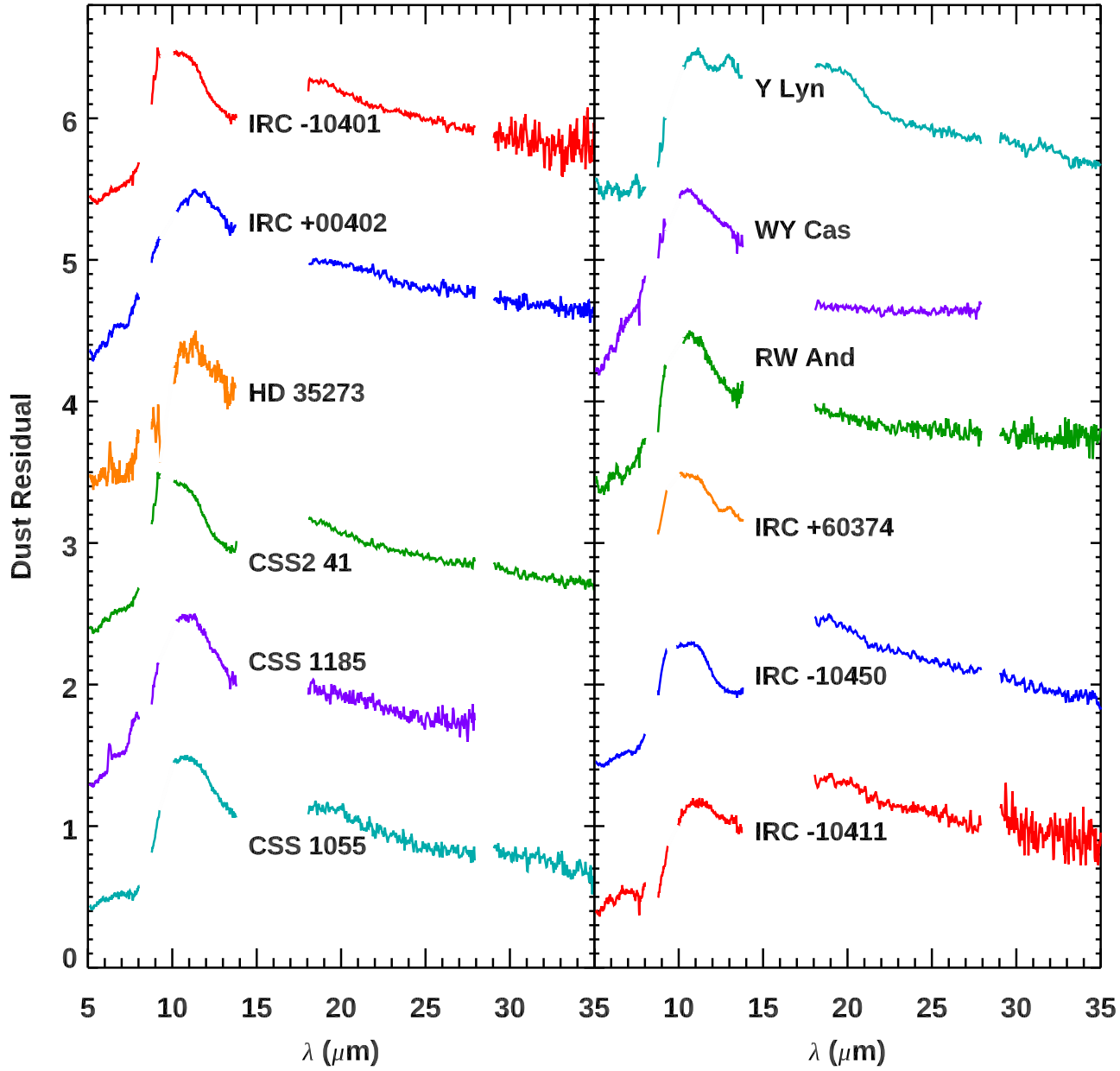

Figure 3. Dust residuals. A stellar continuum was subtracted from each spectrum, the results normalized to the mean residual in G111, and offset for clarity. (The data used to create this figure are available in the online article.)

IRC +00402 (Figure 4, lower-right panel) resembles some of the carbon stars observed with SOFIA by K. E. Kraemer et al. (2019) and would be classed as a CE3 following G. C. Sloan et al. (2016). It is also one of our S stars with a hydrocarbon feature at 6.3 μm, which normal carbon stars do not have.

The 10 μm feature of WY Cas (Figure 4, top-left panel), though, does not resemble either the silicate features of M giants or the SiC features of the carbon stars. It is also one of the sources with no 18 μm feature. Indeed it shows only weak emission in the G229 grating and thus has less cool dust present compared to the other sources, regardless of the mineralogy that causes its odd 10 μm feature.

3.2. Molecular Absorption

Two of the S stars, Y Lyn and RW And, have clear H_2O absorption bands in the 6.5–7.5 μm range. A third star, IRC −10450, has a tentative detection but is too weak to characterize. To isolate the feature in Y Lyn and RW And, we subtract a Planck function from the data. The best temperature was T_{bb} = 1800 K and 1400 K for Y Lyn and RW And, respectively, scaled to the measurements at 6.3–6.4 μm. The result was then converted into absorption as a percentage of the continuum for comparison to the H_2O models. The H_2O absorption models are based on the HITEMP extension of the HITRAN database (L. S. Rothman et al. 1995, 2010) using KSPECTRUM (R. K. Kopparapu et al. 2013; R. M. Ramirez & A. Levi 2018). They were generated at 1500, 2000, and 3000 K, and Figure 5 shows the results. For both stars, the 3000 K model matches the data somewhat better than the cooler models. Choosing a different temperature or normalization range will change the details of the agreement, but in most cases the higher temperature remains the better match compared to the lower-temperature water across most of the wavelength range considered.

Table 2
Feature Summary

Star Name	SE Class	λ_{pk10} (μm)	18 μm?	13 μm?	H_2O	λ_{pk6} (μm)	λ_{c6} (μm)
RW And	4–5, 5	10.7	N	N	~3000 K	...	...
HD 35273	1–3, 4	11.3	...	N	...	6.30	6.34
Y Lyn	3–4t	11.0	Y	Y	~3000 K	...	...
IRC −10401	5–6	<10.1	N	N	...	6.38	6.36
IRC −10411	1–3, 4t:	11.2	Y	Y:	...	...	...
CSS 1055	4, 5	10.8	Y	N	...	...	...
IRC −10450	4–5, 6	10.6	Y	N	weak	...	...
IRC +00402	CE3	11.3	?	N	...	6.30	6.32
CSS2 41	5, 6	<10.1	N	N	...	...	...
CSS 1185	4, 5	10.9	N	N	...	6.28	6.30
IRC +60374	5–6t	<10.2	...	Y	...	...	...
WY Cas	...	10.5	N	N:	...	...	...

Note. SE classes are given for the blue and red sides (if they differ), separated by a comma. IRC +60374 has no continuum subtraction, which could affect the shape and peak wavelength for its 10 μm feature.

This temperature contrasts with the H_2O observed in a set of dust-free M giants, which were better fit by the lower-temperature models 1500 K and 2000 K (G. C. Sloan et al. 2015). A higher temperature could indicate that the absorbing gas is closer to the stellar surface in the S stars. The different abundances of the available oxygen could affect where in the atmosphere the H_2O can condense. Given the noisiness of the spectra and the uncertainty of the fit, this statement should be taken more as guidance than a strong conclusion.

The edge of the SiO absorption band at 7.5 μm was detected in Y Lyn but not in RW And (Figure 2). Y Lyn does have the bluest $K_s - [12]$ color in our sample, although not the bluest [12]−[25]. All but one of the naked (i.e., dust-free) stars in the K. Smolders et al. (2012) sample show SiO, and many also have H_2O absorption (their Figure 4). One star, CSS 783, may have weak H_2O absorption with no SiO feature. Of the dusty S stars in their sample (their Figures 6 and 7), they typically have either both absorption features or neither, and a few only have SiO. Here, too, a single source, CD −392449, may have weak H_2O absorption without the SiO feature.

Thus, RW And seems unusual in having clear H_2O absorption but not SiO absorption. Two additional stars in the Smolders sample may also show this unusual combination, but higher signal-to-noise data are needed to verify it. It is possible that a lack of available oxygen means that the formation of dust has consumed most of the SiO gas, leaving an insufficient amount for the absorption feature to appear in these stars.

3.3. Complex Hydrocarbon Features

Infrared emission features attributed to complex hydrocarbons have frequently been observed in carbon-rich evolved objects such as post-AGB stars and planetary nebulae, typically at wavelengths of ~3.3, 6.2, 7.7–8.6, and 11.3 μm. The features are usually associated with PAHs and related aliphatics (e.g., W. W. Duley & D. A. Williams 1981; A. G. G. M. Tielens 2008), although the detailed composition of their carrier(s) remains the topic of some debate (e.g., S. Kwok 2022). They are generally not seen in carbon stars, as opposed to carbon-rich objects that have evolved beyond the AGB, due to the lack of UV photons to excite the carriers (e.g., A. G. G. M. Tielens 2008). Nonetheless, the features have been detected in cool objects such as red supergiants (e.g., R. J. Sylvester et al. 1994, 1998; T. Verhoelst et al. 2009; O. C. Jones et al. 2017).

3.3.1. Feature Extraction

Three S stars show the hydrocarbon feature at 6.3 μm, CSS 1185, HD 35273, and IRC +00402. In addition, IRC −10401 has a candidate feature. To remove the continuum and isolate the feature, we fit a line to the mean flux levels between 5.95 and 6.05 μm on the blue side and between 6.60 and 6.70 μm on the red side and subtract that from the spectrum, as shown in the left panel of Figure 6. The right panel in the figure shows the residual features for the four stars.

The wavelength at which the feature appears depends slightly on how it is defined. Table 2 gives both λ_{pk}, the peak wavelength and λ_c the wavelength centroid, for each source. The peak wavelength is the wavelength of the peak flux in the continuum-subtracted feature. The wavelength centroid is the wavelength at which half the flux in the continuum-subtracted feature is on either side. These can shift slightly, ~0.01–0.02 μm, depending on the wavelengths chosen, which indicates the uncertainty in the reported wavelengths.

For three of the four stars, the feature appears at $\langle\lambda\rangle = 6.31 \pm 0.02$ μm. This corresponds to "Class C" PAHs, the reddest in the classification scheme of E. Peeters et al. (2002) based on spectra from the SWS (T. de Graauw et al. 1996) on the ISO (M. F. Kessler et al. 1996). The candidate feature in IRC −10401 is even redder, at ~6.37 μm.

The 11.3 μm feature is also commonly observed in spectra with complex hydrocarbon features, including some S stars (K. Smolders et al. 2010). As Figure 7 shows, though, none of the four spectra with 6.3 μm features has a clear emission feature at 11.3 μm. In this spectral region, we used a spline to try and bring out the feature. There is a hint of emission in the three stars with positively identified 6.3 μm features, but that can only be considered tentative; there is no sign of a similar feature for IRC −10401.

The 7.7–8.6 μm complex lies almost entirely in the gap between the G063 and G111 gratings. The spectra for our PAH sources, especially CSS 1185, do show some structure around 7.3–8.0 μm (see Figures 2 or 3). However, the wavelength coverage is insufficient to characterize it or really to distinguish between hydrocarbon emission and the silicate dust feature that is certainly present and beginning to rise.

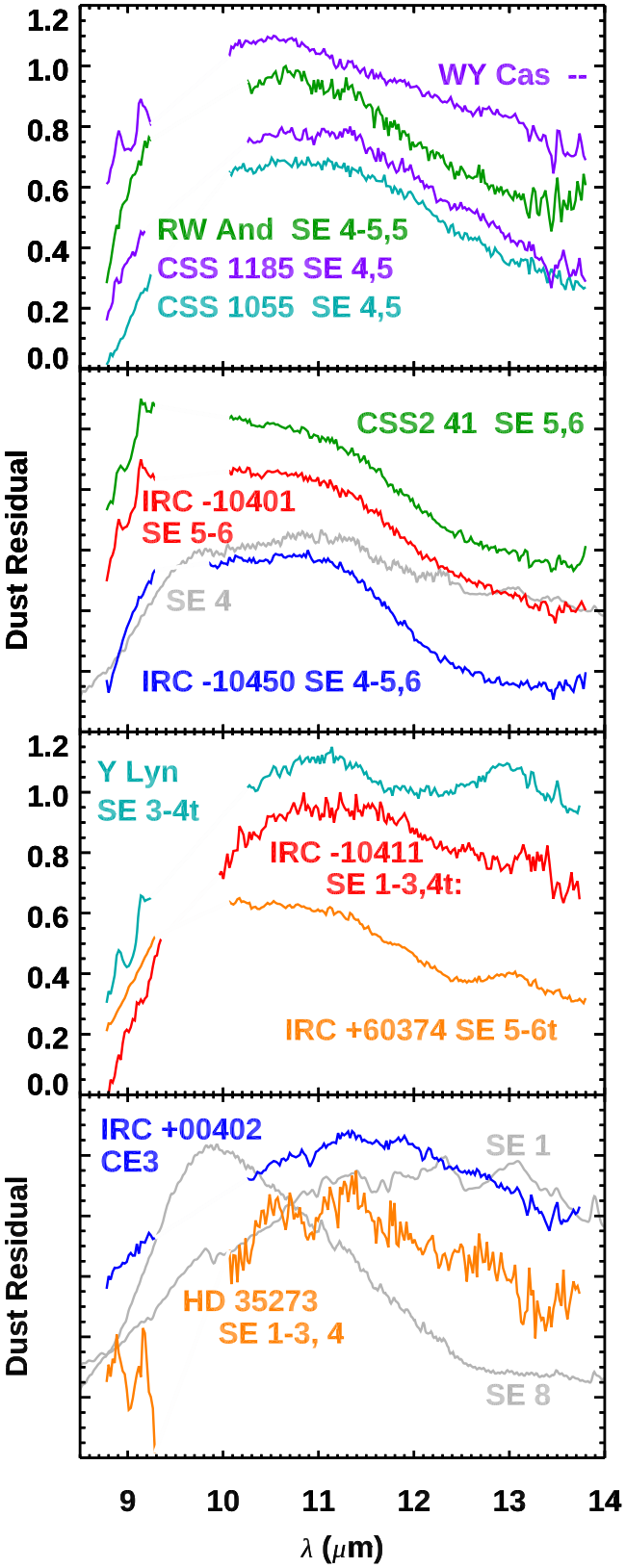

Figure 4. Close-up of the dust features in the 10–11 μm region. Roughly similar spectra are grouped together. SE classes for the blue and red sides are separated by a comma if they differ. The sources with the 13 μm emission feature are in the third panel from the top. Spectra are normalized as described in the text and offset for clarity. Comparison profiles for classes SE 1, 4, and 8 are in gray.

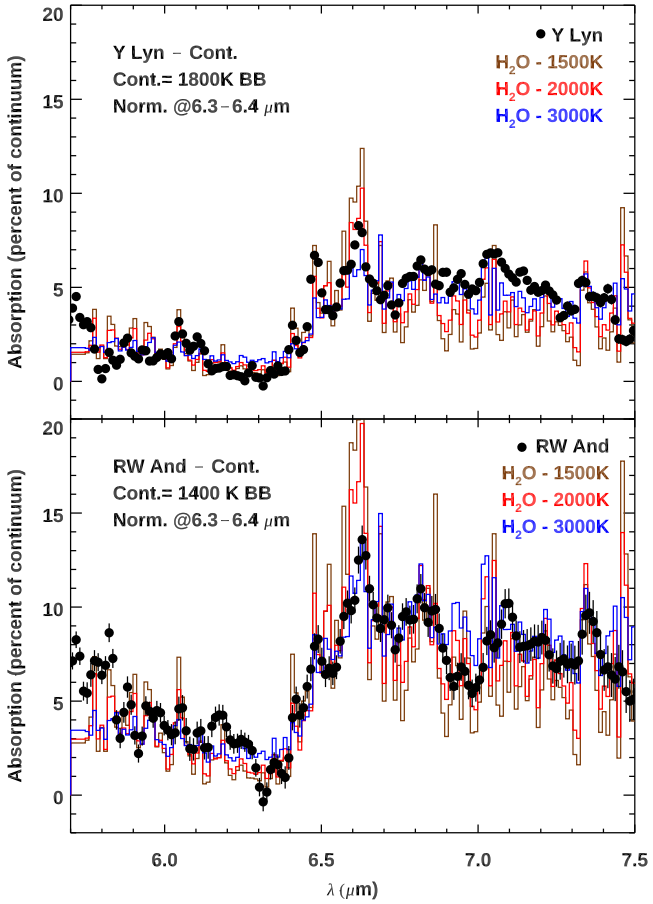

Figure 5. H_2O models from HITEMP compared to (top) Y Lyn and (bottom) RW And. The subtracted continuum is a blackbody function at the given temperature.

(The data used to create this figure are available in the online article.)

3.3.2. Hydrocarbon Excitation

Class C features at 6.3 μm, rather than 6.22–6.28 μm, were originally found in only two carbon-rich post-AGB objects (E. Peeters et al. 2002). Although they have been found in other object types (G. C. Sloan et al. 2014, and references therein), they remain rare compared to the Class A and B sources.

Class C objects generally show a single, broad feature at ~8.0–8.3 μm rather than two distinct features at 7.7 and 8.6 μm (e.g., E. Peeters et al. 2002; P. A. Jensen et al. 2022). G. C. Sloan et al. (2007) note that the 8.6 μm feature does often appear as a bump on the red shoulder of the broader feature in Class C spectra. The 11.3 μm feature is also redder than in Classes A and B.

Three of the four hydrocarbon sources among the S stars of K. Smolders et al. (2010) are also Class C, with a red 6.3 μm feature and broad 8 μm features. Their fourth source has an 11.3 μm feature, but it is Class B in all its PAH features. That is, at least six of the eight S stars with hydrocarbon features are Class C. The candidate 6.3 μm feature in the eighth source, if real, is even redder than Class C.

Class C features are thought to indicate a lack of photo-processing of the molecules. G. C. Sloan et al. (2007) suggested that the wavelength shift from 6.2 to 6.3 μm could be due to the influence of aliphatic bonds relative to aromatics. Laboratory

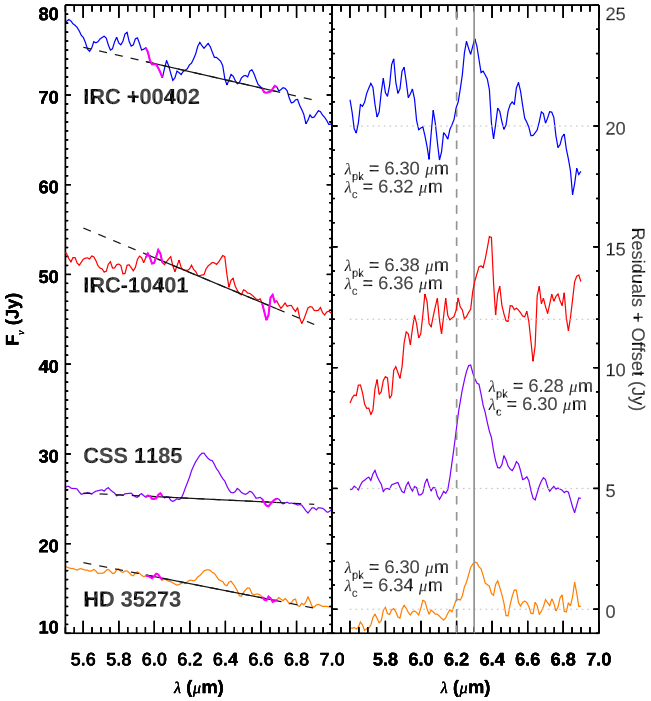

Figure 6. Candidate hydrocarbon features. (left) Continuum fits to the four S stars with the 6.3 μm hydrocarbon feature. (right) Residuals after continuum subtraction, offset for clarity. The vertical lines are at 6.2 and 6.3 μm to guide the eye.

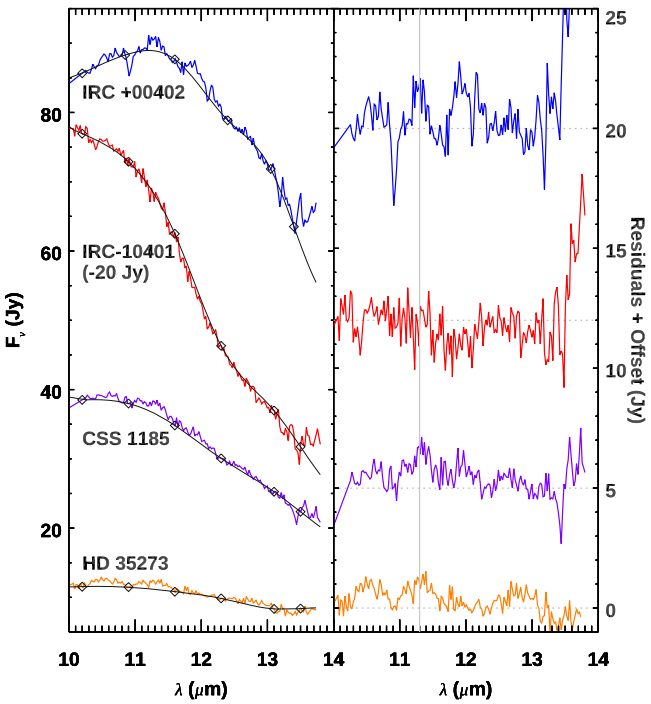

Figure 7. The 11 μm region. (left) Continuum spline fits for the four stars with 6.3 μm features. (right) Residuals after continuum subtraction. The vertical gray line is at 11.3 μm.

measurements of soots by T. Pino et al. (2008) support this scenario. In astrophysical environments, the aliphatics could survive due to the absence of UV radiation, which would certainly be the case for these cool S stars, $T_\star \sim 2000$–3000 K.

The ratio of the 6.2/11.3 μm feature is often used to estimate the charge state of the PAHs, as the 6.2 μm feature is attributed to cations and the 11.3 feature to neutrals (e.g., E. Peeters 2017, and references therein). A weak or absent 11.3 μm feature could indicate high ionization. However, that would conflict with the lack of UV processing indicated by the wavelength shift of the 6.2 μm feature to 6.3 μm. Since a lack of UV radiation is more consistent with the stellar temperatures of S stars, a different explanation for the lack of the 11.3 μm feature is needed here.

The 11.3 μm feature is attributed to a solo C–H out-of-plane bending mode in large, neutral PAHs. An alternate explanation for the absent feature in the S stars is an overabundance of aliphatics rather than aromatics. In this scenario, the hydrogen atoms on the edges of the hydrocarbons are replaced by chains such as methyl or methylene groups. One might expect such a replacement in an aliphatic-rich hydrocarbon mixture, and this could have the effect of suppressing the solo C–H out-of-plane bending mode.

A test of this might be found in the 3–4 μm spectral region, which covers both the aromatic feature at 3.3 μm and the aliphatic feature at 3.4 μm. None of the S stars with the 6.3 μm feature in our sample, though, or that of K. Smolders et al. (2010), have 3 μm spectra. The SWS spectra of the two original Class C post-AGB objects, AFGL 2688 and IRAS 13416 −6243, do extend to 2.4 μm. However, the S/N in these data is insufficient for a definitive test of this scenario. Spectral observations at 3 μm of the S stars themselves are needed to determine the relative abundances of aromatics and aliphatics in these objects.

4. Summary

We observed 12 of the dustiest known S stars in the Milky Way using the FORCAST grisms on SOFIA. All have strong dust emission features in the vicinity of the 10 and 11 μm silicate and SiC features. The shape of the feature in most of the stars, though, is not well matched to the shapes for a single SE class in the scheme often used to categorize dusty oxygen-rich AGB stars. This supports the contention that the dust emission from S stars differs from that in M giants (e.g., I. R. Little-Marenin & S. J. Little 1988; S. Hony et al. 2009). The feature for one star (IRC +00402) is likely due to SiC, indicating its C/O is slightly above 1, and the feature for another star (WY Cas) does not resemble either typical M giant features nor carbon star features.

Two stars show a water absorption band at ∼6.5–7.5 μm, and a third has a tentative detection, but only one of these also has SiO molecular absorption. This combination of water absorption without SiO absorption has only been tentatively seen in two other S stars and is never seen in M giants.

Three stars show the 6.3 μm emission band from complex hydrocarbons, and a fourth may have emission at 6.37 μm, redder than even the class C feature the other three show. None of them show a strong 11.3 μm hydrocarbon emission feature, although the three class C sources have tentative detections. The combination of a red 6.3 μm feature and weak 11.3 μm feature may indicate that aliphatic hydrocarbons are relatively more abundant in these sources compared to the PAHs commonly seen in nebulae. Follow-up observations in the 3.3 μm spectral region would test this possible explanation.

Acknowledgments

We thank the SOFIA flight crew and staff scientists for making these observations, Els Peeters for the helpful discussions on the hydrocarbon emission, and Tom Kuchar for assisting with the photometry. We thank the anonymous referee whose careful reading and thoughtful suggestions have helped improve the paper. This work was based on observations made with the NASA/DLR Stratospheric Observatory for Infrared Astronomy (SOFIA). SOFIA was jointly operated by the Universities Space Research Association, Inc. (USRA), under NASA contract NNA17BF53C, and the Deutsches SOFIA Institut (DSI) under DLR contract 50 OK 0901 to the University of Stuttgart. Financial support for this work was provided by NASA through award SOF09-0046 issued by USRA. We made use of the NASA Astrophysics Data System, IRSA's Gator service, and CDS's Simbad and Vizier services.

Facilities: SOFIA (FORCAST), Spitzer (IRS), ISO (SWS).

Appendix
S Stars Not Observed

Table 3 lists the four S stars in our sample that were not observed by the end of the SOFIA mission.

Table 3
Nonobserved S Stars

Star Name	[12]−[25] (mag)	K_s−[12] (mag)	Spectral Type
TT CMa	0.95	1.94	S
CGCS 4284	1.03	4.59	S
AFGL 2425	1.37	3.57	M10 III
V1959 Cyg	1.30	2.83	S

ORCID iDs

Kathleen E. Kraemer https://orcid.org/0000-0002-2626-7155
G. C. Sloan https://orcid.org/0000-0003-4520-1044
Ramses M. Ramirez https://orcid.org/0000-0001-7553-8444

References

Aoki, W., Tsuji, T., & Ohnaka, K. 1998, A&A, 340, 222
Begemann, B., Dorschner, J., Henning, T., et al. 1997, ApJ, 476, 199
Burbidge, E. M., Burbidge, G. R., Fowler, W. A., & Hoyle, F. 1957, RvMP, 29, 547
Cami, J., Sloan, G. C., Markwick-Kemper, A. J., et al. 2009, ApJL, 690, L122
Cheeseman, P., Stutz, J., Self, M., et al. 1989, NASRP, 1217, 1
Chen, P. S., Liu, J. Y., & Shan, H. G. 2019, AJ, 158, 22
Cutri, R. M., Skrutskie, M. F., van Dyk, S., et al. 2003, 2MASS All Sky Catalog of Point Sources (Pasadena, CA: IPAC)
de Graauw, T., Haser, L. N., Beintema, D. A., et al. 1996, A&A, 315, L49
Duley, W. W., & Williams, D. A. 1981, MNRAS, 196, 269
Egan, M. P., & Sloan, G. C. 2001, ApJ, 558, 165
Habing, H. J. 1996, A&ARv, 7, 97
Hackwell, J. A. 1972, A&A, 21, 239
Herter, T. L., Adams, J. D., De Buizer, J. M., et al. 2012, ApJL, 749, L18
Höfner, S., & Olofsson, H. 2018, A&ARv, 26, 1
Hony, S., Heras, A. M., Molster, F. J., & Smolders, K. 2009, A&A, 501, 609
Iben, I. J. 1974, ARA&A, 12, 215
Iben, I., Jr, & Renzini, A. 1983, ARA&A, 21, 271
Jensen, P. A., Shannon, M. J., Peeters, E., Sloan, G. C., & Stock, D. J. 2022, A&A, 665, A153
Jones, O. C., Woods, P. M., Kemper, F., et al. 2017, MNRAS, 470, 3250
Karakas, A. I., & Lattanzio, J. C. 2014, PASA, 31, e030
Kessler, M. F., Steinz, J. A., Anderegg, M. E., et al. 1996, A&A, 315, L27
Kobayashi, C., Karakas, A. I., & Lugaro, M. 2020, ApJ, 900, 179
Kopparapu, R. K., Ramirez, R., Kasting, J. F., et al. 2013, ApJ, 765, 131
Kraemer, K. E., Sloan, G. C., Keller, L. D., et al. 2019, ApJ, 887, 82
Kraemer, K. E., Sloan, G. C., Price, S. D., & Walker, H. J. 2002, ApJS, 140, 389
Kwok, S. 2022, Ap&SS, 367, 16
Little-Marenin, I. R., & Little, S. J. 1988, ApJ, 333, 305
Matsuura, M., Zijlstra, A. A., van Loon, J. T., et al. 2005, A&A, 434, 691
McDonald, I., Sloan, G. C., Zijlstra, A. A., et al. 2010, ApJL, 717, L92
Merrill, K. M., & Stein, W. A. 1976, PASP, 88, 285
Merrill, P. W. 1926, ApJ, 63, 13
Merrill, P. W. 1929, PA, 37, 444
Mutschke, H., Begemann, B., Dorschner, J., et al. 1998, A&A, 333, 188
Neugebauer, G., Habing, H. J., van Duinen, R., et al. 1984, ApJL, 278, L1
Ossenkopf, V., Henning, T., & Mathis, J. S. 1992, A&A, 261, 567
Peeters, E., Bauschlicher, C. W. J., Allamandola, L. J., et al. 2017, ApJ, 836, 198
Peeters, E., Hony, S., Van Kerckhoven, C., et al. 2002, A&A, 390, 1089
Pegourie, B. 1988, A&A, 194, 335
Pino, T., Dartois, E., Cao, A. T., et al. 2008, A&A, 490, 665
Ramirez, R. M., & Levi, A. 2018, MNRAS, 477, 4627
Rothman, L. S., Gordon, I. E., Barber, R. J., et al. 2010, JQSRT, 111, 2139
Rothman, L. S., Wattson, R. B., Gamache, R., Schroeder, J. W., & McCann, A. 1995, Proc. SPIE, 2471, 105
Ruffle, P. M. E., Kemper, F., Jones, O. C., et al. 2015, MNRAS, 451, 3504
Sloan, G. C., Goes, C., Ramirez, R. M., Kraemer, K. E., & Engelke, C. W. 2015, ApJ, 811, 45
Sloan, G. C., Hony, S., Smolders, K., et al. 2011, ApJ, 729, 121
Sloan, G. C., Jura, M., Duley, W. W., et al. 2007, ApJ, 664, 1144
Sloan, G. C., Kraemer, K. E., Goebel, J. H., & Price, S. D. 2003, ApJ, 594, 483
Sloan, G. C., Kraemer, K. E., McDonald, I., et al. 2016, ApJ, 826, 44
Sloan, G. C., Lagadec, E., Zijlstra, A. A., et al. 2014, ApJ, 791, 28
Sloan, G. C., & Price, S. D. 1995, ApJ, 451, 758
Sloan, G. C., & Price, S. D. 1998, ApJS, 119, 141
Smolders, K., Acke, B., Verhoelst, T., et al. 2010, A&A, 514, L1
Smolders, K., Neyskens, P., Blommaert, J. A. D. L., et al. 2012, A&A, 540, A72
Sylvester, R. J., Barlow, M. J., & Skinner, C. J. 1994, MNRAS, 266, 640
Sylvester, R. J., Skinner, C. J., & Barlow, M. J. 1998, MNRAS, 301, 1083
Takigawa, A., Tachibana, S., Nagahara, H., & Ozawa, K. 2015, ApJS, 218, 2
Tielens, A. G. G. M. 2008, ARA&A, 46, 289
Ulrich, R. K. 1973, in Proc. of the Conf. on Explosive Nucleosynthesis, Explosive Nucleosynthesis, ed. D. N. Schramm & W. D. Arnett (Austin, TX: Univ. Texas Press), 139
Verhoelst, T., van der Zypen, N., Hony, S., et al. 2009, A&A, 498, 127
Wallerstein, G., & Knapp, G. R. 1998, ARA&A, 36, 369
Wright, E. L., Eisenhardt, P. R. M., Mainzer, A. K., et al. 2010, AJ, 140, 1868
Wurm, K. 1940, ApJ, 91, 103
Young, E. T., Becklin, E. E., Marcum, P. M., et al. 2012, ApJL, 749, L17
Zubko, V. G., Mennella, V., Colangeli, L., & Bussoletti, E. 1996, MNRAS, 282, 1321